Materials Research Letters

ISSN: (Print) 2166-3831 (Online) Journal homepage: https://www.tandfonline.com/loi/tmrl20

Study of deformation mechanisms in flash-sintered yttria-stabilized zirconia by *in-situ* micromechanical testing at elevated temperatures

Jaehun Cho, Jin Li, Han Wang, Qiang Li, Zhe Fan, A.K. Mukherjee, W. Rheinheimer, Haiyan Wang & X. Zhang

To cite this article: Jaehun Cho, Jin Li, Han Wang, Qiang Li, Zhe Fan, A.K. Mukherjee, W. Rheinheimer, Haiyan Wang & X. Zhang (2019) Study of deformation mechanisms in flash-sintered yttria-stabilized zirconia by *in-situ* micromechanical testing at elevated temperatures, Materials Research Letters, 7:5, 194-202, DOI: 10.1080/21663831.2019.1575924

To link to this article: https://doi.org/10.1080/21663831.2019.1575924

Published online: 12 Feb 2019.

MATER. RES. LETT.
2019, VOL. 7, NO. 5, 194–202
https://doi.org/10.1080/21663831.2019.1575924

MATERIALS RESEARCH LETTERS
Taylor & Francis
Taylor & Francis Group

ORIGINAL REPORT

Study of deformation mechanisms in flash-sintered yttria-stabilized zirconia by *in-situ* micromechanical testing at elevated temperatures

Jaehun Cho[a], Jin Li[a], Han Wang[a], Qiang Li[a], Zhe Fan [b], A.K. Mukherjee[c], W. Rheinheimer[a], Haiyan Wang [a,d] and X. Zhang [a]

[a]School of Materials Engineering, Purdue University, West Lafayette, IN, USA; [b]Oak Ridge National Laboratory, Oak Ridge, TN, USA; [c]Department of Chemical Engineering & Materials Science, University of California, Davis, CA, USA; [d]School of Electrical and Computer Engineering, Purdue University, West Lafayette, IN, USA

ABSTRACT

Flash sintering has received wide attention lately due to its ultrafast densification process at low sintering temperature. However, the deformability of flash-sintered ceramics remains poorly understood. Yttria-stabilized zirconia (YSZ) was processed by flash sintering to study deformation mechanism. Transmission electron microscopy studies show that the flash-sintered YSZ contains ultrafine grains and dislocations. Strain rate jump tests at elevated temperature by *in-situ* micro-compression indicate the existence of a large threshold stress. The activation energy of deformation is ~145 kJ/mol, similar to the activation energy for oxygen vacancy migration. The deformation mechanisms of the flash-sintered YSZ at elevated temperatures are discussed.

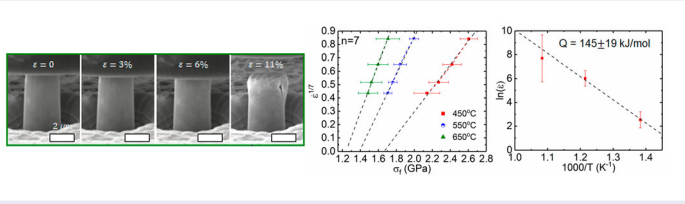

ARTICLE HISTORY
Received 16 July 2018

KEYWORDS
Flash sintering; deformation mechanism; *in-situ* microcompression test; dislocation

IMPACT STATEMENT

The current study reveals the underlying deformation mechanisms of flash-sintered 3YSZ that shows considerable plasticity over the temperature range of 450–650°C via *in-situ* microcompression test.

1. Introduction

Field-assisted sintering technique (FAST) is of great industrial importance and widely applied due to significant energy savings by lowering sintering temperature and time [1]. Flash sintering, one of the FASTs, is a newly developed technique that permits the dramatic reduction of sintering time and temperature and permits substantial currents to flow through specimens [2]. During flash sintering, an ultrafast densification process occurs by applying an electric field at a constant heating rate. When the furnace temperature is higher than the onset (flash) point, which is dependent upon the magnitude of applied electric field and the material's conductivity, an instantaneous densification process takes place within a few seconds [3]. Numerous ceramic systems, such as yttria-stabilized zirconia (YSZ), titania, zinc oxide, and ceria have been successfully prepared by flash sintering [4–7], and the number of flash-sintered ceramic systems increases rapidly. Among these systems, YSZ is one of the most widely explored ceramics in the field of flash sintering, as YSZ has a variety of important industrial applications, such as thermal barrier coatings, dental implants, oxygen sensors, and solid oxide fuel cells [8–11].

Mechanical behavior of YSZ has been intensively investigated. There are several studies on microscale mechanical testing, which mostly highlight superior superelasticity and shape memory effect at room temperature owing to martensitic transformation [12–18]. However, our understanding on deformation mechanisms of microscale YSZ at elevated temperatures remains lim-

CONTACT Haiyan Wang hwang00@purdue.edu School of Materials Engineering, Purdue University, West Lafayette, IN 47907, USA; School of Electrical and Computer Engineering, Purdue University, West Lafayette, IN 47907, USA; X. Zhang xzhang98@purdue.edu School of Materials Engineering, Purdue University, West Lafayette, IN 47907, USA

Supplemental data for this article can be accessed here. https://doi.org/10.1080/21663831.2019.1575924

ited. In addition, ceramics processed by flash sintering technique is known to have intriguing microstructures containing a considerable number of charged defects and ultrafine grain sizes [3,19]. Our previous *in-situ* study shows that the flash-sintered YSZ has a high density of preexisting dislocations induced by flash sintering and has a transition of deformation mechanisms at 400°C [20]. Here, we report further studies on the underlying deformation mechanisms of the flash-sintered 3 mol% yttria doped zirconia (3YSZ) at elevated temperatures (above 400°C). We utilize *in-situ* microcompression jump tests to avoid complicated data analyses associated with nanoindentation [21]. These tests reveal the existence of a large threshold stress for activation of dislocation creep. Furthermore, the activation energy for creep is measured from *in-situ* compression tests and provides important insight on defect dominated deformation mechanisms in flash-sintered ceramics.

2. Experimental procedures

The experiment was conducted in a customized thermomechanical analyzer (SETSYS Evolution, SET ARAM Instrumentation). Disk-shaped 3YSZ specimens with a diameter of $\sim$5 mm and a thickness of $\sim$2 mm (using TZ-3Y-E powders, from Tosoh corp., with 40 nm grain size, please see Table S1 for purity information.) were sandwiched between two Pt electrodes. An alumina rod pushed the electrodes with a few kPa pressure to insure a rigid contact between the sample and electrodes. A compact specimen dimension was intentionally used to minimize density and grain size fluctuations throughout the sample. An electrical field of 150 V/cm was applied to the specimen with a constant heating rate of 25°C/min until the sample undergoes a rapid densification at a furnace temperature of 1150°C. Right after the onset of flash, the applied heat and electric field were removed right away to prohibit grain growth.

Transmission electron microscopy (TEM) studies were performed on the as-sintered 3YSZ. Sequential grinding, polishing, dimpling and ion milling (PIPS II, Gatan) were employed to manually prepare TEM specimens of the flash-sintered 3YSZ. TEM experiments were performed on an FEI Talos 200X transmission electron microscope operated at 200 kV.

To investigate the microscale mechanical behavior of flash-sintered 3YSZ, micropillars with $\sim$3 μm in diameter and $\sim$8 μm in height were fabricated by focused ion beam (FIB) technique in an FEI 3D FEG and Zeiss 1540 XB dual-beam scanning electron microscope. The pillars were prepared on a dense area (judged by SEM studies) and thus the pillars from this region contain only a few nanovoids as can be seen in Figure 1(c) and (d). The specimen was mounted on a ceramic stage heater in a Hysitron PI 88 × R nanoindentation system. A 5 μm diameter diamond flat punch tip equipped on a piezoelectric transducer for collection of force and displacement was used to compress the micropillars. The diamond flat punch and specimen were heated to desired temperatures (450°C, 550°C, and 650°C) at the same ramping rate of 20°C/min. The microcompression tests were conducted when thermal equilibrium is achieved to minimize mechanical and thermal drifts. Thermal drift rate, less than 1.1 nm/s, was measured prior to each compression tests for 40 s. True displacement data compensating the displacement offset were acquired by the nanoindentation system.

3. Results

TEM micrograph (Figure 1(a)) shows ultrafine grain size in the flash-sintered 3YSZ. A systematic linear intercept method reveals the average grain size (more than 200 grains) of 159 ± 70 nm with a large variation, and the flash-sintered 3YSZ has a 98% density determined by many micrographs. TEM studies also show a significant amount of preexisting dislocations (Figure 1(b)). Strain rate jump tests were carried out on numerous micropillars at different temperatures (450°C, 550°C, and 650°C) to study the underlying deformation mechanisms. A strain rate of $5 \times 10^{-4}\,s^{-1}$ was applied in the elastic region ($\sim$2%) of the stress–strain curve, and strain rates of $3 \times 10^{-3}\,s^{-1}$, $1 \times 10^{-2}\,s^{-1}$, $5 \times 10^{-2}\,s^{-1}$, and $3 \times 10^{-1}\,s^{-1}$ were applied in the plastic deformation region to obtain flow stresses at each temperature. Figure 1(c–e) shows SEM snapshots of the tested pillars at various strains at each temperature. Cracks propagated downwards from top surface, but no catastrophic failure was observed after tests at elevated temperatures. Figure 2(a–c) shows multiple stress–strain curves of strain rate jump tests at three temperatures. The stress–strain behavior shows good reproducibility taking into consideration the porous nature of ceramic materials. As test temperature increases, the flow stresses tend to decrease, and crack density and propagation speed reduce significantly. The flow stresses for each strain rate were obtained at a strain of 6%, which is half of the maximum compression strain (12%). Such a strain value permits the least extrapolation for stress analysis at each strain rate. Also, every stress–strain curve collected at three temperatures shows the obvious stress plateau above 4% to 5% strain, indicating that the strain from which the flow stresses is collected should be larger than 5% strain.

The flow stresses at various temperatures and strain rates were extracted and plotted as a function of strain rate after taking natural logarithm (Figure S1(a)). Strain

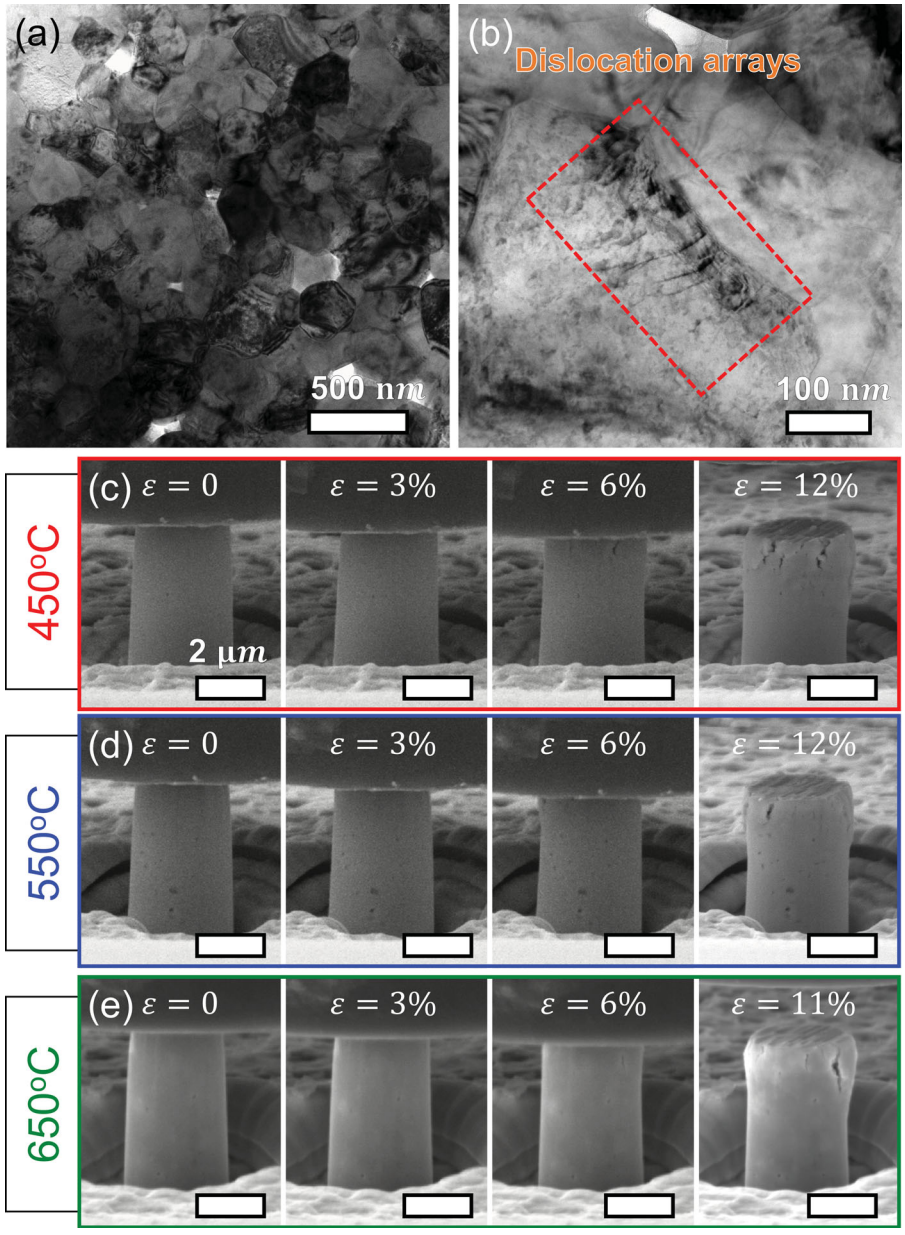

Figure 1. Microstructure and strain rate jump tests on the flash sintered 3YSZ. (a–b) Bright field TEM micrographs of the flash sintered 3YSZ showing (a) ultrafine grains and (b) an array of preexisting dislocations. (c–e) SEM snapshots of the pillars tested at 450°C, 550°C, and 650°C at 0, 3%, 6%, and final strains (11–12%). Several cracks propagated from the top surface of the pillar. Crack length and density reduce as test temperature rises.

rate sensitivity (m) at a fixed temperature and strain can be calculated by

$$m = \left(\frac{\partial \ln \sigma}{\partial \ln \dot{\varepsilon}}\right)_{\varepsilon,T}, \tag{1}$$

where σ is an applied stress and $\dot{\varepsilon}$ is strain rate [22]. m values obtained from the slope of the fitting line in Figure S1(a) at 450°C, 550°C, and 650°C are 0.043 ± 0.022, 0.034 ± 0.011, and 0.030 ± 0.030, respectively. The deformation mechanism of materials at elevated temperature follows an Arrhenius-type relation under the assumption that the deformation is dominated by a single process [23] and can be expressed by

$$\dot{\varepsilon} = A_o \sigma^n \exp\left(-\frac{Q}{RT}\right), \tag{2}$$

where A_o is the pre-exponential constant, n is the stress exponent, and Q is activation energy of the dominant deformation mechanism. When we assume the constant stress exponent and applied stress, Equation (2) can be rewritten as

$$\dot{\varepsilon} = A_1 \exp\left(-\frac{Q}{RT}\right), \tag{3}$$

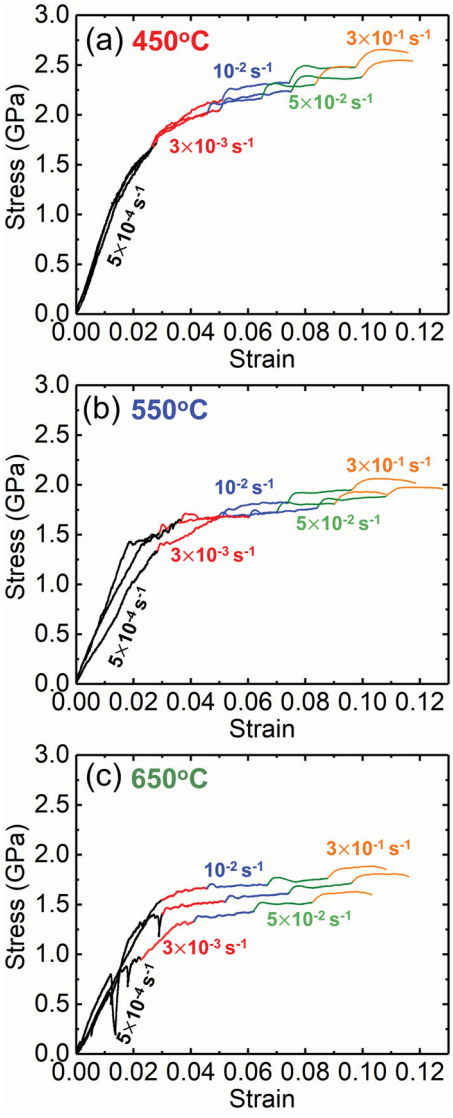

Figure 2. Stress–strain curves for strain rate jump tests on the flash sintered 3YSZ at 450, 550, and 650°C. Stress–strain curves for three strain rate jump tests at (a) 450°C, (b) 550°C, and (c) 650°C. Strain rate of $5 \times 10^{-4}\ s^{-1}$ was employed in the elastic region. Strain rates of $3 \times 10^{-3}\ s^{-1}$, $1 \times 10^{-2}\ s^{-1}$, $5 \times 10^{-2}\ s^{-1}$, and $3 \times 10^{-1}\ s^{-1}$ were utilized in the plastic region to obtain flow stresses at each temperature. The flow stresses increase with increasing strain rate and decreasing temperature.

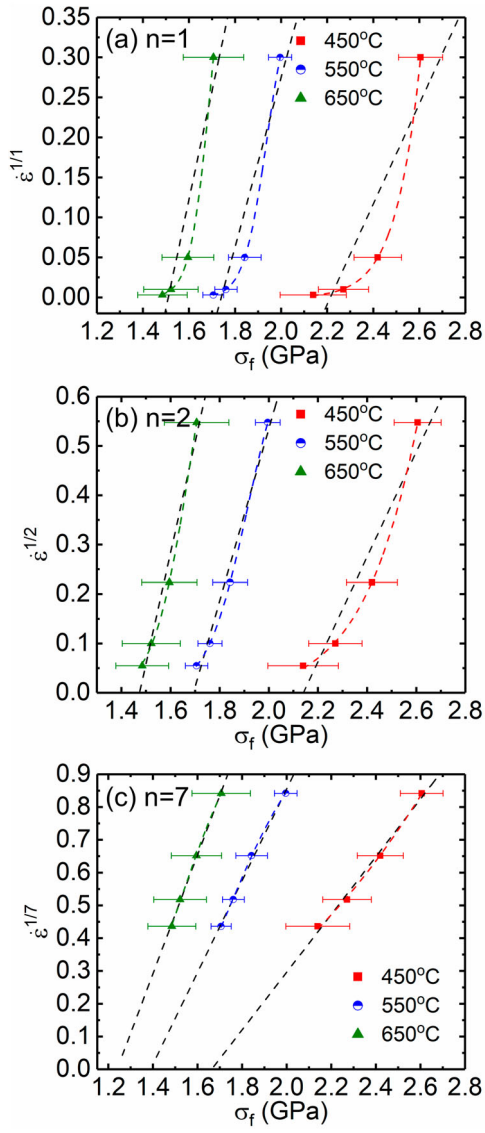

Figure 3. The determination of the threshold stress for the flash sintered 3YSZ at 450°C, 550°C, and 650°C. (a) The determination of the threshold stress with a stress exponent of 1. The actual data points deviate significantly from the linear regression lines as indicated by the curved dash lines. (b) The determination of the threshold stress with a stress exponent of 2. The actual data shows better linear fit than those with a stress exponent of 1, but still deviates from the linear regression lines by exhibiting positive upward curvature. (c) The determination of the threshold stress with a stress exponent of 7. The linear regression lines match well with the actual data. The extrapolation of the linear line to zero strain rate describes the threshold stress.

where A_1 is a constant, which includes the applied stress term [24]. The assumption of the constant stress exponent for the power law means that there is no transition in deformation mechanisms within the test temperatures in agreement with our previous study [25]. When the applied stress is fixed at 2000 MPa, the corresponding strain rates can be obtained at each temperature by drawing a horizontal line in Figure S1(a). By plotting $\ln \dot{\varepsilon}$ vs. 1000/T, the activation energy can be calculated from the slope (Figure S1(b)). The activation energy so calculated is 347 ± 151 kJ/mol. Plotting $\ln(\dot{\varepsilon} \exp(Q/RT))$ vs. $\ln \sigma$ with a substitution of the activation energy of 347 kJ/mol into Equation (1) yields an unusually large stress exponent of ~ 30 (Figure S1(c)). The unphysically high-stress exponent obtained using this method implies that threshold stress must be taken into account for exploring the underlying deformation mechanism. The threshold stress, σ_o, can be graphically determined

by plotting $\dot{\varepsilon}^{1/n}$ vs. σ at each temperature and is used to correct the stress in Equation (2) as follows:

$$\dot{\varepsilon} = A_o(\sigma - \sigma_o)^n \exp\left(-\frac{Q}{RT}\right). \quad (4)$$

The threshold stress is determined from the intercept between the linear regression of extrapolated data points and the stress axis (when $\dot{\varepsilon} = 0$) as demonstrated in Figure 3. To determine the threshold stress, the stress exponent must be known. The most common deformation mechanisms of YSZ system are diffusional creep ($n = 1$), grain boundary sliding ($n = 2$) and dislocation creep ($n = 7$) [26,27]. Figure 3(a–c) shows $\dot{\varepsilon}^{1/n}$ vs. σ plot when we assume that the dominant deformation mechanism is diffusional creep, or grain boundary sliding, or dislocation creep, respectively. When the stress exponent is assumed to be 1, the fitting of data points significantly deviates from the linear regression (dotted lines), indicating that $n = 1$ is an unlikely scenario. Similarly, the assumption of $n = 2$ also leads to a noticeable deviation from the linear regression line. When $n = 7$ is assumed, the linear regression lines exhibit best fits for data points at all three test temperatures. Such an observation indicates that the same deformation mechanism takes place during this temperature range, and thus justifies the assumption of a constant stress exponent in Equation (3). Therefore, the threshold stresses at each temperature were obtained from the linear extrapolation of the experimental data using $n = 7$. The data were replotted in Figure 4 after taking the effective stress $(\sigma - \sigma_o)$ into account. Plotting $\ln(\sigma - \sigma_o)$ vs. $\ln\dot{\varepsilon}$ in Figure 4(a) shows corrected strain rate sensitivities of 0.155 ± 0.085, 0.142 ± 0.050, and 0.154 ± 0.151 at 450°C, 550°C, and 650°C, respectively. The corrected activation energy of 145 ± 74 kJ/mole was obtained at a constant flow stress of 500 MPa by plotting $\ln\dot{\varepsilon}$ vs. 1000/T. The strain rate sensitivities become much greater and the activation energy significantly decreases after the correction of the flow stress. The determination of the threshold stresses with an imposed stress exponent of 7 naturally returns a self-consistent stress exponent of 6.7 as demonstrated in Figure 4(c).

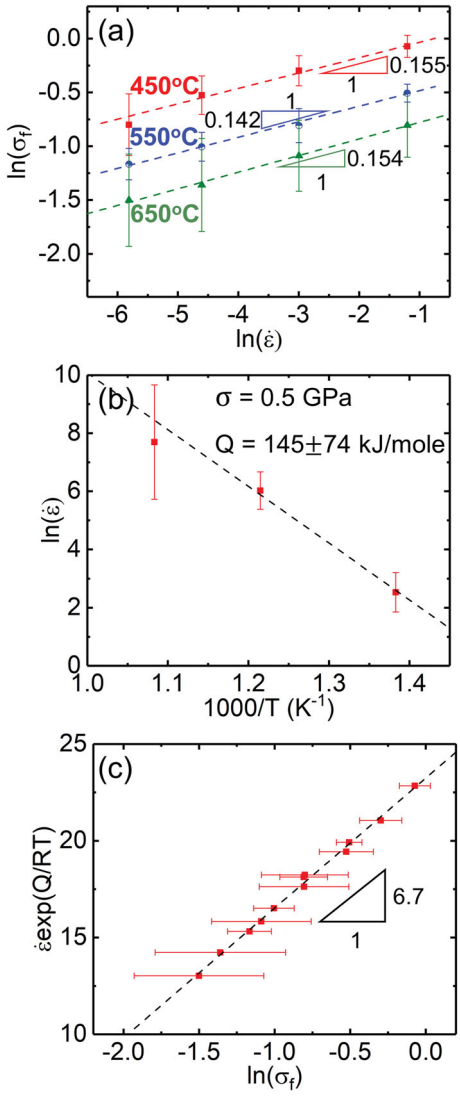

Figure 4. Corrected data processing from strain rate jump tests on the flash sintered 3YSZ at 450°C, 550°C, and 650°C in consideration of the presence of the threshold stress. (a) The corrected flow stress as a function of strain rates at each temperature. The strain rate sensitivities after the correction increase to 0.15. (b) Temperature dependence of strain rate at a flow stress of 500 MPa. The activation energy is estimated to be 145 ± 74 kJ/mole. (c) The corrected flow stress versus the normalized strain rate. The data correction with an imposed stress exponent of 7 returns the stress exponent of 6.7.

4. Discussion

A majority of ceramic materials have little dislocations, unless deformed at high temperatures. Prior studies on flash-sintered 3YSZ show that arrays of dislocations are retained frequently, and some dislocations exist near the triple junctions where the sintering stress is concentrated during the flash sintering process [20]. This noticeable presence of high-density dislocations in the flash-sintered 3YSZ is surprising. It has been shown that flash sintering can induce a significant amount of point defects in ceramics [19]. We anticipate that substantial mass transport during flash sintering results in considerable plastic flow, which is accommodated by generation and migration of a high-density of dislocations [3]. We also hypothesize that during flash sintering, the transient high current densities through specimens along with locally very high temperatures due to Joule heating promote sintering and introduce a significant number

of defects, such as Frenkel defects [2], dislocations, and stacking faults. The formation or nucleation of these defects facilitate the plastic deformation of the flash sintered YSZ. The activity of dislocations may not play a significant role in the deformability of 3YSZ at room temperature as the glide of dislocations is often hindered by the strong covalent and ionic bonding. However, the nucleation and activity of dislocations in bulk 3YSZ were often observed after mechanical tests at high temperatures (> 800°C) [28,29]. In the current study, abundant intragranular dislocations and entanglement were already generated by the high strain rate mass flow during fast densification process. Furthermore, the plastic deformation of ceramics by dislocation glide in micromechanical tests has been observed previously because the miniaturization of specimen decreases strain gradients and the population of intrinsic flaws [30–32]. Therefore, it is likely that the abundant preexisting dislocations contribute to the deformability of the flash-sintered 3YSZ at the intermediate test temperatures. One may speculate that the high concentration of defects (dislocations and point defects) may be unstable and tends to decrease significantly at high temperatures. However, in the present *in-situ* experiments, the test temperatures are relatively low, ranging from 450°C to 650°C, which are equivalent to 0.27–0.31T_m. At these temperatures, the mobility (i.e. diffusion coefficients) of cationic point defects is negligible. As such, a defect equilibration involving a diffusion of cationic defects is less likely to occur for kinetic reasons. Also, the intermediate temperature is insufficient for recovery of dislocations in ceramics.

Initial plots of the experimental data from the strain rate jump tests, following Equation (1), yield the stress exponent of 30, too high to physically describe the appropriate deformation mechanisms. Such an abnormally large n value has been reported before, and the introduction of threshold stress as shown in Equation (4) returns a more appropriate n value and activation energy [33–35]. Following a similar methodology, the linear regression of the data using a n value of 7 provides the best linear fit as evidenced in Figure 3(c). Furthermore, the usage of a modified creep equation returns a self-consistent n value of 6.7, indicating the methodology applied here is appropriate. An n value of 7 corresponds to dislocation glide dominated creep mechanism. Thus, the current study suggests that the dislocation activity may be the dominant deformation mechanism in the flash-sintered 3YSZ between 450 and 650°C. This temperature range is lower than the onset of dislocation controlled creep in conventional YSZ, which typically is higher than 800°C.

The threshold stresses obtained from the intercept of the linear extrapolation with the stress axis are 1.67, 1.39, and 1.24 GPa for tests at 450, 550, and 650°C, respectively. The threshold stress of ~1.7 GPa is abnormally large to be explained by using the conventional concept of grain-boundary dislocations and surface tensions. As such, the introduction of friction stress can help to understand the large threshold stresses determined here. It is known that materials with high Peierls stress tend to have large errors in activation energies and stress exponents when calculated using conventional creep equations [36]. Therefore, the introduction of σ_o, referred to as internal stress or friction stress, in the creep equations is necessary to obtain appropriate values [37]. Given that YSZ is a ceramic material, its high Peierls stress in this study is not very surprising. Kamimura et al. [38] suggested Equation (5) yielding Peierls stress (τ_p) for 3YSZ via Peierls–Nabarro model of the planar core dislocation.

$$\tau_P = \mu k \frac{b}{\delta} \exp\left(-k\pi \frac{h}{\delta}\right) \quad \text{and}$$
$$k = \frac{1}{2\pi}\left(\frac{\sin^2\theta}{1-\nu} + \cos^2\theta\right), \tag{5}$$

where μ is the shear modulus, k is an preexponential factor, b is the Burgers vector, δ is the lattice periodicity, h is the spacing of the glide plane, θ is the angle between dislocation line and Burgers vector, and ν is the Poisson's ratio. Their equation yields the maximum value of 6.4 GPa for 3YSZ at 450°C, higher than the threshold stress obtained in this study. Baufeld et al. derived Peierls stress of 4.5 GPa for fully stabilized zirconia (doped with 11 mol% Y_2O_3) at 600°C using experimental data [39]. Dominguez-Rodriguez et al. determined the friction stress of 2.4 GPa for 9.4 mol% YSZ at < 570°C [40]. We believe that the segregated oxygen vacancies at the dislocation core in the flash sintered 3YSZ reduces the Peierls (friction) stress by decreasing the strength of interatomic bonds.

The threshold stresses observed in metallic materials are typically measured at high temperature, where sometimes superplasticity has been observed in, e.g. Al alloys [35]. Furthermore, the threshold stress appears to decrease at higher test temperature. In this study, higher test temperature may weaken the strong covalent and ionic bonding of 3YSZ, such that the threshold stress decreases as temperature increases. Furthermore, the calculated threshold stresses are comparable to the yield strength of specimens at each temperature as shown in Table 1. As such, we hypothesize that the large threshold stress in this study is (1) the stress necessary to activate the migration of dislocations or (2) the stress necessary to overcome the friction caused by the point defects segregated along the dislocation cores. In general, the yield strength of polycrystalline ceramic materials indicates

Table 1. Flow stress, yield strength and threshold stress at each temperature and strain rate.

Temperature (°C)	Strain rate (s^{-1})	Flow stress (GPa)	Yield strength (GPa)	Threshold stress (GPa)
450	0.003	2.14 ± 0.14	1.32 ± 0.25	1.67 ± 0.05
	0.01	2.27 ± 0.11		
	0.05	2.42 ± 0.10		
	0.3	2.61 ± 0.10		
550	0.003	1.71 ± 0.05	1.19 ± 0.10	1.39 ± 0.02
	0.01	1.76 ± 0.05		
	0.05	1.84 ± 0.07		
	0.3	2.00 ± 0.05		
650	0.003	1.48 ± 0.11	1.07 ± 0.13	1.24 ± 0.11
	0.01	1.52 ± 0.12		
	0.05	1.60 ± 0.11		
	0.3	1.71 ± 0.13		

the stress necessary for microcracking, phase transformation, or dislocation movement [41]. It was reported that dislocation dominated plastic flow is favorable at the low homologous temperature and high external stress [42]. The highest test temperature in this *in-situ* study is equivalent to $0.31T_m$ and the applied external stress is higher than 1 GPa. On the other hand, the high threshold stress may also be related to segregation of charged point defects along the dislocation cores, exerting a pinning effect that can be explained by interpretation of the activation energy shown in the next paragraph.

The activation energy for the rate controlling mechanism is $\sim$145 kJ/mol after taking the presence of threshold stress into consideration. Such a value is significantly less than the activation energy for grain boundary diffusion and lattice diffusion of cations, but comparable to the activation energy for oxygen and oxygen vacancy migration (96.5–220 kJ/mol) in YSZ (See Table 2) [47–51]. As will be discussed in the following, it seems likely that this low activation energy is a consequence of point defect segregation to the dislocations and their pinning and dragging impact due to diffusion. When assumed that the migration of dislocations is governed by thermal activation required to overcome local obstacles (point defects in our hypothesis) and/or friction stress, we can estimate the activation energy of dislocation movement by adopting the classical dislocation theory (See the Supplementary Information for details). Impurity segregation to dislocations is a well-known phenomenon in the metallic materials and is known to be analogous to grain boundary segregation [52–54]. Such segregation can pin dislocations and hinder their motion. However, if these segregates have a suitable diffusion coefficient, they might be dragged along with migrating dislocations, causing a solute drag effect [55–58] again analogous to solute drag on grain boundary motion [59]. The same concept applies to ceramic materials, although segregation is also related to electrostatics as defects now involve charges [60–63]. As such, dislocation lines can have a charge causing additional driving force for their segregation. Around the dislocation line, complementary charge accumulates to compensate the charge of the dislocations, analogous to space charges at grain boundaries [60,63]. As mobile segregates (point defects) cause a solute drag for dislocations, the diffusion of point defects would be the rate limiting step for dislocation movement. In the case of YSZ, segregations of Y and O to the grain boundaries have been reported [64]. In the present in-situ experiments up to 650°C, cationic defects are largely immobile in YSZ. However, oxygen (and oxygen vacancy) diffusion in YSZ is known to have very high diffusion coefficients [65]. As such, it is likely that the migration of dislocations in YSZ involves the diffusion of segregated oxygen or oxygen vacancies. The agreement of the measured activation energy of dislocation migration (145 kJ/mole) with oxygen or oxygen vacancy diffusion (96.5–220 kJ/mole) supports this hypothesis.

Table 2. Activation energy of grain boundary and lattice diffusion for Zr, Y, O, and oxygen vacancy (V_o).

	Grain boundary diffusion (kJ/mole)	Lattice diffusion (kJ/mole)
Cations (Zr, Y)	370 [43]	460–650 [44–46]
O	188 [47]	220 [47]
V_o	–	96.5–164 [48–51]

5. Conclusions

In summary, 3YSZ was processed by the flash sintering technique under an electric field of 150 V/cm. *In-situ* microcompression tests on the flash sintered 3YSZ was performed at 450–650°C to study the underlying deformation mechanism. Strain rate jump tests lead to a stress exponent of $\sim$7, and threshold stresses comparable to the yield strengths. The calculated activation energy of 145 kJ/mol is comparable to the activation energy for oxygen vacancy migration. This study suggests that the abundant defects induced during flash sintering (oxygen vacancies and dislocations) lead to improved plasticity, and the deformation mechanism may be dislocation glide and climb assisted by oxygen vacancy migration over the temperature range of 450–650°C for the flash-sintered 3YSZ. This study sheds lights on the mechanical behavior of an important class of ceramic materials that have widespread industrial applications.

Acknowledgements

We acknowledge accesses to Life Science Microscopy Facility and the microscopy center of School of Materials Engineering at Purdue University. We also acknowledge the access of microscopy center at the Center for Nanoscale Materials at

Argonne National Laboratory, an Office of Science User Facility, which was supported by the U. S. Department of Energy, Office of Science, Office of Basic Energy Sciences, under Contract No. DE-AC02-06CH11357.

Disclosure statement

No potential conflict of interest was reported by the authors.

Funding

This work is primarily supported by the U.S. Office of Naval Research [grant number N00014-17-1-2087] (sample preparation and *in-situ* SEM), [grant number N0014-16-1-2778] (TEM). QL is supported by Department of Energy BES [grant number DE-SC0016337].

ORCID

Zhe Fan http://orcid.org/0000-0001-6223-6228
Haiyan Wang http://orcid.org/0000-0002-7397-1209
X. Zhang http://orcid.org/0000-0002-8380-8667

References

[1] Guillon O, Gonzalez-Julian J, Dargatz B, et al. Field-assisted sintering technology/spark plasma sintering: mechanisms, materials, and technology developments. Adv Eng Mater. 2014;16:830–849.
[2] Cologna M, Rashkova B, Raj R. Flash sintering of nanograin zirconia in < 5 s at 850°C. J Am Ceram Soc. 2010;93:3556–3559.
[3] Jha SK, Terauds K, Lebrun J, et al. Beyond flash sintering in 3 mol% yttria stabilized zirconia. J Ceram Soc Japan. 2016;124:283–288.
[4] Cologna M, Prette ALG, Raj R. Flash-sintering of cubic yttria-stabilized zirconia at 750°C for possible use in SOFC manufacturing. J Am Ceram Soc. 2011;94:316–319.
[5] Jha SK, Raj R. The effect of electric field on sintering and electrical conductivity of titania. J Am Ceram Soc. 2014;97:527–534.
[6] Charalambous H, Jha SK, Lay RT, et al. Investigation of temperature approximation methods during flash sintering of ZnO. Ceram Int. 2018;44(6):1–8.
[7] Li J, Guan L, Zhang W, et al. Sintering behavior of samarium doped ceria under DC electrical field. Ceram Int. 2018;44:2470–2477.
[8] Padture NP. Thermal barrier coatings for gas-turbine engine applications. Science (80). 2012;280:280–285.
[9] Kelly JR, Denry I. Stabilized zirconia as a structural ceramic: an overview. Dent Mater. 2008;24:289–298.
[10] Ramamoorthy R, Dutta PK, Akbar SA. Oxygen sensors: materials, methods, designs. J Mater Sci. 2003;38:4271–4282.
[11] Tao S, Irvine JTS. A redox-stable efficient anode for solid-oxide fuel cells. Nat Mater. 2003;2:320–323.
[12] Lai A, Du Z, Gan CL, et al. Shape memory and superelastic ceramics at small scales. Science (80-). 2013;341:1505–1508.
[13] Du Z, Zeng XM, Liu Q, et al. Size effects and shape memory properties in ZrO_2 ceramic micro- and nano-pillars. Scr Mater. 2015;101:40–43.
[14] Zeng XM, Lai A, Gan CL, et al. Crystal orientation dependence of the stress-induced martensitic transformation in zirconia-based shape memory ceramics. Acta Mater. 2016;116:124–135.
[15] Camposilvan E, Anglada M. Size and plasticity effects in zirconia micropillars compression. Acta Mater. 2016;103:882–892.
[16] Zeng XM, Du Z, Schuh CA, et al. Microstructure, crystallization and shape memory behavior of titania and yttria co-doped zirconia. J Eur Ceram Soc. 2016;36:1277–1283.
[17] Du Z, Zeng XM, Liu Q, et al. Superelasticity in micro-scale shape memory ceramic particles. Acta Mater. 2017;123:255–263.
[18] Cho J, Li J, Li Q, et al. In-situ high temperature micromechanical testing of ultra fine grained yttria-stabilized zirconia processed by spark plasma sintering. Acta Mater. 2018;155:128–137.
[19] Narayan J. A new mechanism for field-assisted processing and flash sintering of materials. Scr Mater. 2013;69:107–111.
[20] Wang H, Phuah X, Li J, et al. Key microstructural characteristics in flash sintered 3YSZ critical for enhanced sintering process. Ceram. Int. 2019;45(1):1251–1257.
[21] Carpenter JS, Misra A, Uchic MD, et al. Strain rate sensitivity and activation volume of Cu/Ni metallic multilayer thin films measured via micropillar compression. Appl Phys Lett. 2012;101:051901.
[22] Wei Q, Cheng S, Ramesh KT, et al. Effect of nanocrystalline and ultrafine grain sizes on the strain rate sensitivity and activation volume: Fcc versus bcc metals. Mater Sci Eng A. 2004;381:71–79.
[23] Mukherjee AK. The rate controlling mechanism in superplasticity. Mater Sci Eng. 1971;8:83–89.
[24] Zhang X, Wang H, Scattergood RO, et al. Studies of deformation mechanisms in ultra-fine grained and nanostructured zinc. Acta Mater. 2002;50:4823–4830.
[25] Cho J, Li Q, Wang H, et al. High temperature deformability of ductile flash sintered ceramics via in-situ compression. Nat Commun. 2018;9:2063.
[26] Balasubramanian N, Langdon TG. Flow processes in superplastic yttria-stabilized zirconia: a deformation limit diagram. Mater Sci Eng A. 2005;409:46–51.
[27] Charit I, Chokshi AH. Experimental evidence for diffusion creep in the superplastic 3 mol% yttria-stabilized tetragonal zirconia. Acta Mater. 2001;49:2239–2249.
[28] Morita K, Hiraga K. Reply to "comment on the role of intragranular dislocations in superplastic yttria-stabilized zirconia". Scr Mater. 2003;48:1402–1407.
[29] Morita K, Hiraga K. Deformed substructures in fine-grained tetragonal zirconia. Philos Mag Lett. 2001;81:311–319.
[30] Korte S, Barnard JS, Stearn RJ, et al. Deformation of silicon - insights from microcompression testing at 25–500°C. Int J Plast. 2011;27:1853–1866.
[31] Montagne A, Pathak S, Maeder X, et al. Plasticity and fracture of sapphire at room temperature: load-controlled microcompression of four different orientations. Ceram Int. 2014;40:2083–2090.

[32] Kiani S, Leung KWK, Radmilovic V, et al. Dislocation glide-controlled room-temperature plasticity in 6H-SiC single crystals. Acta Mater. 2014;80:400–406.
[33] Mishra RS, Mukherjee AK. On superplasticity in silicon carbide reinforced aluminum composites. Scr Metall Mater. 1991;25:271–275.
[34] Mishra RS, Bieler TR, Mukherjee AK. On the superplastic behaviour of mechanically alloyed aluminum alloys. Scr Metall Mater. 1992;26:1605–1608.
[35] Mishra RS, Bieler TR, Mukherjee AK. Superplasticity in powder metaluurgy aluminum alloys and composites. Acta Metall Mater. 1995;43:877–891.
[36] Mitchell TE, Hirth JP, Misra A. Apparent activation energy and stress exponent in materials with a high Peierls stress. Acta Mater. 2002;50:1087–1093.
[37] Mitchell TE, Heuer AH. Dislocations and mechanical properties of ceramics. Dislocations in solids. New York: Elsevier B.V.; 2005.
[38] Kamimura Y, Edagawa K, Iskandarov AM, et al. Peierls stresses estimated via the Peierls-Nabarro model using ab-initio γ-surface and their comparison with experiments. Acta Mater. 2018;148:355–362.
[39] Baufeld B, Petukhov B V, Bartsch M, et al. Transition of mechanisms controlling the dislocation motion in cubic ZrO_2 below 700°C. Acta Mater. 1998;46:3077–3085.
[40] Dominguez-Rodriguez A, Heuer AH, Castaing J. Dislocations and the mechanical properties of stabilized ZrO_2. Radiat Eff Defects Solids. 1991;119–1212:759–769.
[41] Lankford J, Predebon WW, Staehler JM, et al. The role of plasticity as a limiting factor in the compressive failure of high strength ceramics. Mech Mater. 1998;29:205–218.
[42] Ashby MF, Verrall RA. Diffusion-accommodated flow and superplasticity. Acta Metall. 1973;21:149–163.
[43] Sakka Y, Oishi Y, Ando K. Zr-Hf interdiffusion in polycrystalline Y_2O_3-$(Zr+Hf)O_2$. J Mater Sci. 1982;17:3101–3105.
[44] Dimos D, Kohlstedt DL. Diffusional creep and kinetic demixing in yttria-stabilized zirconia. J Am Ceram Soc. 1987;70:531–536.
[45] Jiménez-Melendo M, Domínguez-Rodríguez A, Bravo-León A. Superplastic flow of fine-grained yttria-stabilized zirconia polycrystals: constitutive equation and deformation mechanisms. J Am Ceram Soc. 1998;81:2761–2776.
[46] Hiraga K, Yasuda HY, Sakka Y. The tensile creep behavior of superplastic tetragonal zirconia doped with small amounts of SiO_2. Mater Sci Eng A. 1997;234–236:1026–1029.
[47] Brossmann U, Knöner G, Schaefer HE, et al. Oxygen diffusion in nanocrystalline ZrO_2. Rev Adv Mater Sci. 2004;6:7–11.
[48] Wakiya N, Tajiri N, Kiguchi T, et al. Activation energy of oxygen vacancy diffusion of yttria-stabilized-zirconia thin film determined from DC current measurements below 150°C. Japanese J Appl Physics, Part 2 Lett. 2006;45:L525–L528.
[49] Dong Y, Chen I. Onset criterion for flash sintering. J Am Ceram Soc. 2015;3627:3624–3627.
[50] Todd RI, Bonilla RS, Sneddon T, et al. Electrical characteristics of flash sintering: thermal runaway of Joule heating. J Eur Ceram Soc. 2015;35:1865–1877.
[51] Ramamoorthy R, Sundararaman D, Ramasamy S. Ionic conductivity studies of ultrafine-grained yttria stabilized zirconia polymorphs. Solid State Ionics. 1999;123:271–278.
[52] Kirchheim R. Reducing grain boundary, dislocation line and vacancy formation energies by solute segregation. I. Theoretical background. Acta Mater. 2007;55:5129–5138.
[53] Kirchheim R. Reducing grain boundary, dislocation line and vacancy formation energies by solute segregation. II. Experimental evidence and consequences. Acta Mater. 2007;55:5139–5148.
[54] Miller MK. Atom probe tomography characterization of solute segregation to dislocations. Microsc Res Tech. 2006;69:359–365.
[55] Fuentes-samaniego R, Gasca-Neri R, Hirth JP. Solute drag on moving edge dislocations. Philos Mag A Phys Condens Matter Struct Defects Mech Prop. 1984;49:31–43.
[56] Yoshinaga H, Morozumi S. The solute atmosphere round a moving dislocation and its dragging stress. Philos Mag. 1971;23:1367–1385.
[57] Wang Y, Srolovitz DJ, Rickman JM, et al. Dislocation motion in the presence of diffusing solutes: a computer simulation study. Acta Mater. 2000;48:2163–2175.
[58] Gittus JH. Theoretical equation for steady state dislocation creep: effect of solute drag. Acta Metall. 1974;22:1179–1181.
[59] Cahn JW. The impurity-drag effect in grain boundary motion. Acta Metall. 1962;10:789–798.
[60] Lartigue-Korinek S, Carry C, Priester L. Multiscale aspects of the influence of yttrium on microstructure sintering and creep of alumina. J Eur Ceram Soc. 2002;22:1525–1541.
[61] Nerikar PV, Casillas Trujillo LA, Andersson DA, et al. Segregation of xenon to dislocations and grain boundaries in uranium dioxide. Phys Rev B. 2011;84:174105.
[62] Suzuki T, Ueno M, Nishi Y, et al. Dislocation loop formation in nonstoichiometric (Ba, Ca) TiO_3 and $BaTiO_3$ ceramics. J Am Ceram Soc. 2001;84:200–206.
[63] Sun L, Marrocchelli D, Yildiz B. Edge dislocation slows down oxide ion diffusion in doped CeO_2 by segregation of charged defects. Nat Commun. 2015;6:1–10.
[64] Feng B, Lugg NR, Kumamoto A, et al. Direct observation of oxygen vacancy distribution across yttria-stabilized zirconia grain boundaries. ACS Nano. 2017;11:11376–11382.
[65] Badwall SPS. Zirconia-based solid electrolytes: microstructure, stability and ionic conductivity. Solid State Ionics. 1992;52:23–32.